THE JOURNAL OF BIOLOGICAL CHEMISTRY VOL. 281, NO. 12, pp. 8197–8204, March 24, 2006

Regulation of the Monomer-Dimer Equilibrium in Inducible Nitric-oxide Synthase by Nitric Oxide*[S]

Received for publication, July 6, 2005, and in revised form, January 17, 2006 Published, JBC Papers in Press, January 18, 2006, DOI 10.1074/jbc.M507328200

David Li[‡1], Eric Y. Hayden[‡], Koustubh Panda[§], Dennis J. Stuehr[§], Haiteng Deng[¶], Denis L. Rousseau[‡2], and Syun-Ru Yeh[‡3]

From the [‡]Department of Physiology and Biophysics, Albert Einstein College of Medicine of Yeshiva University, Bronx, New York 10461, the [§]Department of Immunology, Lerner Research Institute, Cleveland Clinic, Cleveland, Ohio 44195, and the [¶]Proteomics Resource Center, Rockefeller University, New York, New York 10021

The oxygenase domain of inducible nitric-oxide synthase exists as a functional tight homodimer in the presence of the substrate L-arginine and the cofactor tetrahydrobiopterin (H4B). In the absence of H4B, the enzyme is a mixture of monomer and loose dimer. We show that exposure of H4B-free enzyme to NO induces dissociation of the loose dimer into monomers in a reaction that follows single exponential decay kinetics with a lifetime of ~300 min. It is followed by a faster autoreduction reaction of the heme iron with a lifetime of ~30 min and the concurrent breakage of the proximal iron–thiolate bond, forming a five-coordinate NO-bound ferrous species. Mass spectrometry revealed that the NO-induced monomerization is associated with intramolecular disulfide bond formation between Cys^{104} and Cys^{109}, located in the zinc-binding motif. The regulatory effect of NO as a dimer inhibitor is discussed in the context of the structure/function relationships of this enzyme.

Nitric-oxide synthase (NOS)[4] catalyzes the formation of NO from oxygen and L-Arg via a consecutive two-step reaction using NADPH as the electron source (1–3). In the first step of the reaction, L-Arg is hydroxylated to *N*-hydroxyarginine; and in the second step, *N*-hydroxyarginine is oxidized to citrulline and NO. The three major isoforms, inducible NOS (iNOS), endothelial NOS, and neuronal NOS (found in macrophages, endothelial cells, and neuronal tissues, respectively), produce NO that functions as a cytotoxic agent, a vasodilator, and a neurotransmitter, respectively (4). The homodimeric enzyme consists of a reductase domain, which binds FMN, FAD, and NADPH, and an oxygenase domain, which binds the heme and tetrahydrobiopterin (H4B) cofactors. During catalysis, electrons flow from NADPH through FMN and FAD in the reductase domain of one subunit of the homodimer to the oxygenase domain of the other subunit (5, 6). The crystal structures of the oxygenase domain of all three isoforms have been determined (7–10). They show that the heme is coordinated by a cysteine residue on the proximal side, as in cytochrome P450-type enzymes, and that the substrate (L-Arg or *N*-hydroxyarginine) binds above the heme iron atom in the distal pocket, whereas the cofactor (H4B) binds along the side of the heme.

It is well accepted that dimerization is essential for NOS function (1, 11). The heme group, the H4B cofactor, and the substrate have all been shown to contribute to dimer stability (12–16). In iNOS, the N-terminal region (between residues 76 and 111, comprising a β-hairpin hook and a *CXXXC* zinc-binding motif) is also believed to be important for stabilizing the dimeric structure. Crane *et al.* (17) reported that the N-terminal region of the iNOS oxygenase domain ($iNOS_{oxy}$) can be in either a "swapped" or an "unswapped" conformation, as illustrated in Fig. 1. In the unswapped conformation, Cys^{104} and Cys^{109} in the zinc-binding motif of each subunit of the dimer are tetrahedrally coordinated to a single zinc ion at the dimer interface, and the β-hairpin hook interacts primarily with its own subunit; in the swapped conformation, Cys^{109} forms a self-symmetric disulfide bond across the dimer interface, and the β-hairpin hook in one subunit of the dimer interacts primarily with the other subunit across the interface (17). Crane *et al.* proposed that the conformational switch between the two structures may play an important role in NOS stability and function in *vivo*.

It has been found that NO produced from the catalytic reaction in iNOS not only can rebind to the heme iron, thereby directly inhibiting the turnover of the enzyme (18, 19), but also can induce monomerization of the functional dimers (16). Although binding of L-Arg and H4B to iNOS promotes the formation of a "tight" dimer, which is resistant to monomerization by NO, it has been shown that the NO-induced monomers cannot be reverted back to the dimeric state by the addition of L-Arg and H4B (16). The dimer inhibition function of NO has also been reported in endothelial NOS by Ravi *et al.* (20), who discovered that exogenous NO induces *S*-nitrosylation of a Cys residue in the zinc-binding motif, thereby reducing the dimer level and the associated enzymatic activity. Another type of dimer inhibition function of NO in iNOS has been demonstrated in the RAW 264.7 mouse macrophage cell line by Albakri and Stuehr (21), who found that NO produced by iNOS induced by cytokines limits the intracellular assembly of iNOS into the dimeric form by preventing heme insertion and decreasing heme availability.

Although it is clear that NO plays an important role in regulating the monomer-dimer equilibrium, the molecular mechanism underlying the NO-induced structural transition remains poorly understood. Here, we systematically studied the interaction between NO and wild-type $iNOS_{oxy}$ as well as two mutants (D92A and K82A) by optical absorption and resonance Raman spectroscopies; in addition, the chemical modi-

* This work was supported in part by National Institutes of Health Grants CA53914 and GM51491 (to D. J. S.), HL65465 (to S.-R. Y.), and GM54806 (to D. L. R.). The costs of publication of this article were defrayed in part by the payment of page charges. This article must therefore be hereby marked "*advertisement*" in accordance with 18 U.S.C. Section 1734 solely to indicate this fact.

[S] The on-line version of this article (available at http://www.jbc.org) contains supplemental Figs. S1–S7.

[1] Supported by Medical Scientist Training Program Grant GM07288 and Molecular Biophysics Training Grant GM08572 from the National Institutes of Health.

[2] To whom correspondence may be addressed: Dept. of Physiology and Biophysics, Albert Einstein College of Medicine of Yeshiva University, Ullman 325, 1300 Morris Park Ave., Bronx, NY 10461. Tel.: 718-430-4264; Fax: 718-430-8808; E-mail: rousseau@aecom.yu.edu.

[3] To whom correspondence may be addressed: Dept. of Physiology and Biophysics, Albert Einstein College of Medicine of Yeshiva University, 1300 Morris Park Ave., Bronx, NY 10461. Tel.: 718-430-4234; Fax: 718-430-4230; E-mail: syeh@aecom.yu.edu.

[4] The abbreviations used are: NOS, nitric-oxide synthase; iNOS, inducible nitric-oxide synthase; H4B, tetrahydrobiopterin; NOS_{oxy}, nitric-oxide synthase oxygenase domain; EPPS, 4-(2-hydroxyethyl)-1-piperazinepropanesulfonic acid; PAR, 4-(2-pyridylazo)resorcinol monosodium salt; 6C, six-coordinate; 5C, five-coordinate.

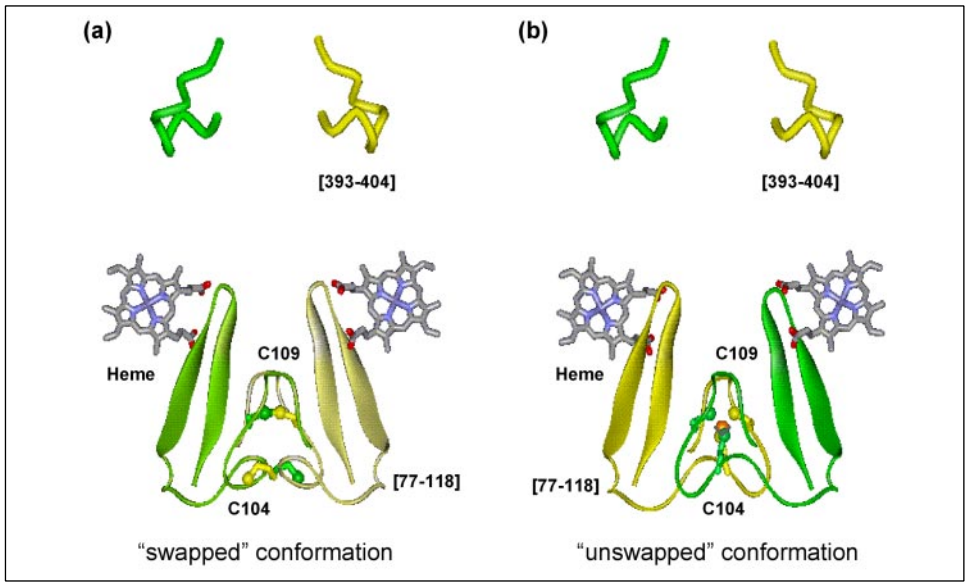

FIGURE 1. **Crystal structures of dimeric H4B-bound iNOS$_{oxy}$.** *a*, the swapped structure (Protein Data Bank code 1QOM) with an intermolecular disulfide bond between the Cys^{109} residues from each subunit; *b*, the unswapped structure (Protein Data Bank code 1DF1) with a zinc (shown as an *orange sphere*) coordinated by Cys^{104} and Cys^{109} from each subunit. Cys^{104} and Cys^{109} are labeled in ball-and-stick representation. The important peptide segments of the two subunits located in the dimer interface are shown in *yellow* and *green*.

fications of the protein matrix induced by NO were examined by mass spectrometry. The data reveal a detailed mechanism of the inhibitory and regulatory effects of NO, as a heme iron ligand, a cysteine-modifying agent, and an inhibitor of dimerization.

MATERIALS AND METHODS

(6*R*)-5,6,7,8-Tetrahydro-L-biopterin was purchased from Alexis Biochemicals (San Diego, CA). All other reagents were from Sigma. Murine wild-type iNOS$_{oxy}$ and mutants were expressed in *Escherichia coli*, purified, and prepared as described previously (17, 22). For urea-containing samples, urea was added from a 12 M stock solution and allowed to equilibrate for 3 h prior to the measurements. To form the NO-bound complexes, 400 μl of 1 atm NO was injected into N_2-purged solutions sealed in an optical cuvette. All spectroscopic measurements were made under anaerobic conditions.

Optical Absorption and Resonance Raman Measurements—Optical absorption and resonance Raman spectra were obtained as described previously (22). For these measurements, the protein was kept in 40 mM EPPS at pH 7.6. The concentrations used are listed in the figure legends. The time-dependent optical spectra were deconvoluted using a program written with Mathcad software (Mathsoft, Cambridge, MA). In each case, the reference for the six-coordinate NO-bound species was taken immediately after the addition of NO. The reference spectrum for the five-coordinate species for all fittings was taken following incubation of the 4 M urea-treated sample with NO for >15 h. The kinetic traces were fitted using commercial software (Origin, RockWare, Golden, CO).

Mass Spectrometric Measurements—The NO-treated iNOS$_{oxy}$ samples were generated by incubating the enzyme with NO for 12 h under anaerobic conditions at room temperature. The reaction was quenched by purging the NO with argon gas. All samples were then digested aerobically with modified trypsin (sequence-grade; Promega Corp.) in ammonium bicarbonate buffer overnight at 37 °C. All digestion products were desalted, separated by gradient elution with a Dionex reverse phase capillary/nano high pressure liquid chromatography system, and analyzed using an Applied Biosystems QSTAR XL tandem mass spectrometer with the hybrid quadrupole time-of-flight configuration. IDA (information-dependent acquisition) software was employed for automatic acquisition of mass spectrometric and tandem mass spectrometric data. The iNOS$_{oxy}$ sample without NO treatment was used as a control. To test the presence of disulfide bonds, half of the digestion products of the urea-treated sample were treated with 10 mM dithiothreitol in 0.1 M ammonium bicarbonate to reduce possible disulfide bonds; the free cysteine residues were then alkylated with freshly prepared iodoacetamide (55 mM in 0.1 M ammonium bicarbonate buffer); and the resulting sample was subsequently subjected to the mass spectrometric analysis.

Size Exclusion Chromatographic Analysis—The Superdex 200 10/30 GL column was purchased from Amersham Biosciences. The iNOS samples (100 μl of 10–20 μM) were incubated first with 50 μM H4B and 5 mM L-Arg for >3 h and then with 0–7 M urea for 3 h. They were loaded onto the column pre-equilibrated with 40 mM EPPS at pH 7.6 at the specified concentrations of urea. The flow rate was 0.35 ml/min for all measurements, which were carried out at 4 °C, and the samples were run for 1.5 column volumes.

The PAR Zinc Chelation Assay—4-(2-Pyridylazo)resorcinol monosodium salt (PAR) was purchased from Sigma. The zinc content was measured by the PAR assay as described previously (23) with slight modifications. The iNOS$_{oxy}$·NO complex was prepared as described above. PAR was added to yield a final concentration of 8 μM. As a control, PAR was added to a ferric iNOS$_{oxy}$ sample at the same concentration. To isolate the contributions in the spectra from PAR in ferric iNOS$_{oxy}$ plus PAR and iNOS$_{oxy}$·NO plus PAR, the corresponding iNOS$_{oxy}$ spectra were subtracted.

RESULTS

To evaluate the effect of NO on the dimeric interactions in iNOS$_{oxy}$, the substrate- and cofactor-free ferric enzyme was subjected to NO, and the reactions were monitored by optical absorption spectroscopy as a function of time. As shown in Fig. 2*a*, immediately after the addition of NO, a species with a Soret absorption maximum at 439 nm and visible absorption bands at 549 and 580 nm was produced. It was assigned as a six-coordinate (6C) NO-bound ferric iNOS$_{oxy}$ complex because its spectra are analogous to those of other reported 6C NO-bound NOS complexes (24). The 6C NO-bound ferric enzyme gradually converted to a species with a Soret maximum at ~390 nm over an ~300-min time period with a clear isosbestic point at 411 nm. The new species was assigned as a five-coordinate (5C) derivative of iNOS$_{oxy}$ because its spectral properties are similar to those of other 5C derivatives of NOS (22, 24). The properties of the 5C species are discussed below. To fur-

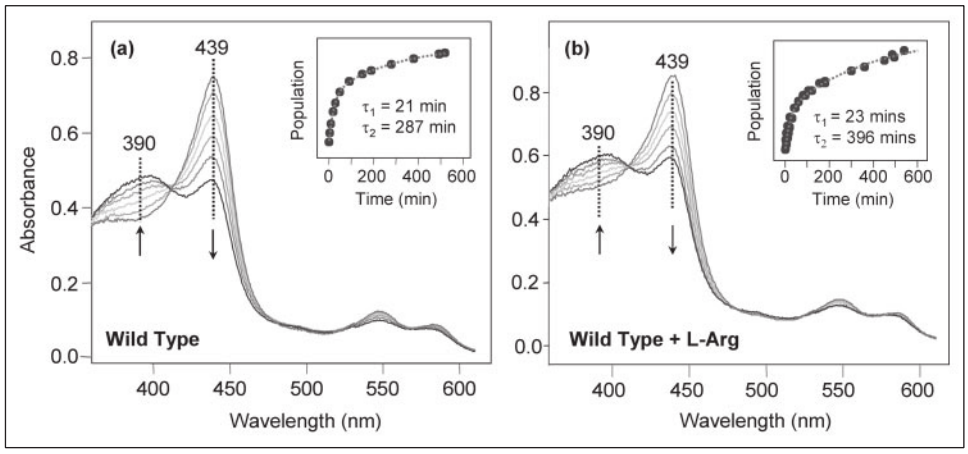

FIGURE 2. **Optical absorption spectra of the H4B- and dithiothreitol-free ferric form of $iNOS_{oxy}$ in the absence (*a*) and presence (*b*) of L-Arg (10 mM) as a function of time following exposure to ~1 mM NO.** The *arrows* indicate the direction of absorbance changes with increasing time. *Insets*, the relative populations of the 5C NO-bound species as a function of time on the basis of spectral deconvolution of the time-dependent optical absorption data. The *dotted lines* show double exponential fits of the data. The relative amplitudes of the fast to the slow phases are 51/49 in *a* and 33/67 in *b*. The concentrations of the $iNOS_{oxy}$ samples were 100 and 90 μM in *a* and *b*, respectively.

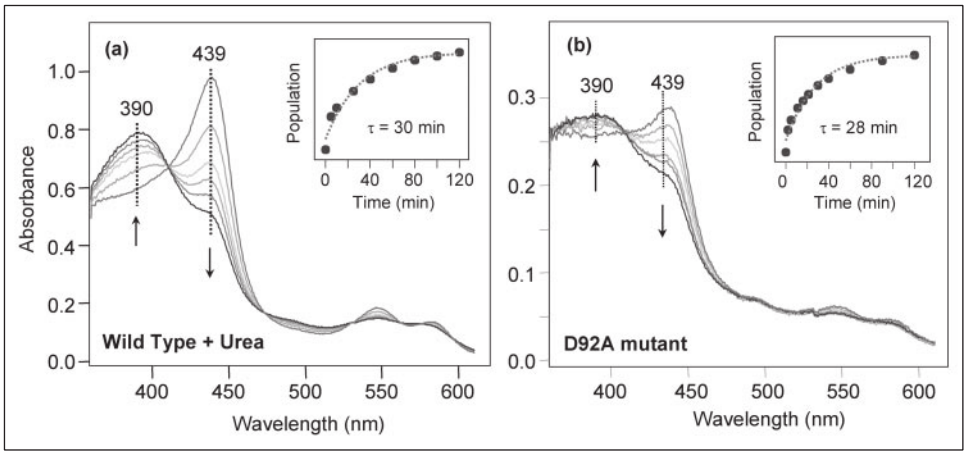

FIGURE 3. **Optical absorption spectra of the 4 M urea-treated sample (*a*) and the D92A mutant (*b*) of H4B- and dithiothreitol-free ferric $iNOS_{oxy}$ as a function of time following exposure to ~1 mM NO.** The *arrows* indicate the direction of absorbance changes with increasing time. *Insets*, the relative populations of the 5C NO-bound species as a function of time on the basis of spectral deconvolution of the time-dependent optical absorption data. The *dotted lines* show single exponential fits of the data. The concentrations of the $iNOS_{oxy}$ samples were 100 and 30 μM in *a* and *b*, respectively.

ther evaluate the mechanism of the 6C-to-5C conversion, we deconvoluted each time-dependent spectrum into a linear combination of the spectrum of the 6C NO-bound ferric species and that of the 5C species. Typical examples demonstrating the reliability of the deconvolution process are shown in supplemental Fig. S1. The resulting population of the 5C species is plotted as a function of time in Fig. 2*a* (*inset*), and the associated kinetic trace was best fit with a double exponential function with lifetimes of 21 and 287 min. A similar reaction was observed for $iNOS_{oxy}$ in the presence of L-Arg as shown in Fig. 2*b*. Although the kinetic lifetimes (23 and 396 min) were only slightly altered upon the addition of L-Arg, the relative amplitude of the slow phase increased from 49% in the absence of L-Arg to 67% in its presence.

The conversion of the 6C NO-bound ferric derivative to the 5C species was inhibited by the binding of H4B, either with or without L-Arg (supplemental Fig. S2). On the basis of gel filtration analysis, Panda and co-workers (15) have reported that, in the absence of H4B, $iNOS_{oxy}$ is in equilibrium between a monomeric form and a "loose" dimeric form and that L-Arg binding shifts the equilibrium toward the loose dimer, whereas H4B binding generates a tight dimer. Accordingly, we postulated that the production of the 5C species in the reaction shown in Fig. 2 was a consequence of the lack of strong dimeric interactions in the absence of H4B. We attribute the slow phase to the reaction of the loose dimer because the amplitude of the slow phase increased from 49 to 67% when L-Arg was added, and we attribute the fast phase to the reaction of the monomeric fraction of the $iNOS_{oxy}$ samples because it decreased correspondingly in the presence of L-Arg.

To test this hypothesis, we examined the reaction between the monomeric form of $iNOS_{oxy}$ and NO using a urea-induced monomer as a model. It has been reported that 5 M urea induces 100% conversion of the dimeric enzyme into monomers, but it is accompanied by significant loss of the heme group because of denaturation; on the other hand, reducing the urea concentration to 3 M can induce only ~94% of the dimer to convert to its monomeric form (15). To find the best conditions for generating the monomeric enzyme without denaturation, we titrated $iNOS_{oxy}$ with urea and found that 4 M urea was an optimum condition for generating the monomeric enzyme without heme loss (supplemental Fig. S3*a*). The monomeric state of the 4 M urea-treated $iNOS_{oxy}$ sample was confirmed by MALDI-TOF mass spectrometric measurements (data not shown) and by gel filtration analysis (supplemental Fig. S4). As shown in Fig. 3*a*, exposure of 4 M urea-treated $iNOS_{oxy}$ to NO instantaneously produced a 6C NO-bound ferric species with a Soret maximum at 439 nm, just as observed in the urea-free samples shown in Fig. 2; in addition, an analogous spectral transition from the 6C NO-bound ferric derivative to a 5C species was observed, although with altered kinetics. To gain quantitative information, the population of the 5C species was estimated by spectral deconvolution of the optical absorption data and was plotted as a function of reaction time in Fig. 3*a* (*inset*). The resulting kinetic trace was best fit with a single exponential function with a lifetime of ~30 min. This lifetime is similar to that of the fast phase (21–23 min) obtained in the absence of urea (Fig. 2), consistent with the scenario that the fast phase originates from the monomeric enzyme. It should be noted that, in the gel filtration measurements in 4 M urea, a small amount of dimer was detected, but its elution volume was spread out compared with that in the absence

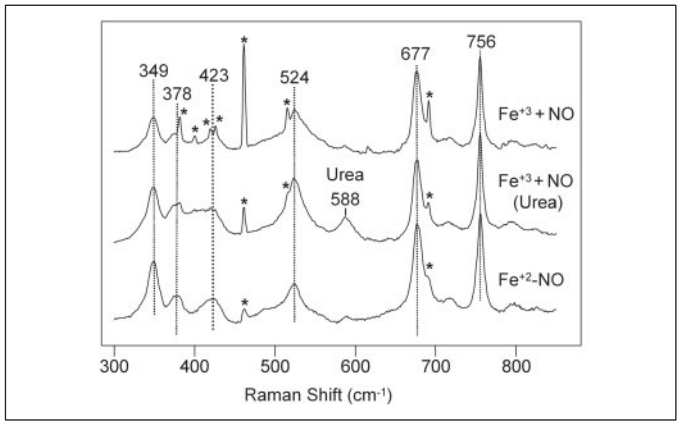

FIGURE 4. **Resonance Raman spectra of the 5C NO-bound species generated from the ferric derivative of $iNOS_{oxy}$ in the absence and presence of 4 M urea and the 5C NO-bound ferrous derivative.** All spectra were obtained at an excitation wavelength at 406.7 nm. The *asterisks* denotes the plasma lines from the laser. The vibrational mode at 588 cm^{-1} is associated with urea.

of urea. We attribute it to some very loose dimer, which reacted with NO as rapidly as the monomer.

To further confirm that the fast phase indeed originates from the monomeric derivative and to eliminate any possible side effects caused by the addition of urea, the NO reaction was examined using two $iNOS_{oxy}$ mutants (D92A and K82A) that adopt a pure monomeric conformation in the absence of H4B (25). Fig. 3*b* shows the time-dependent optical absorption spectra of the D92A mutant of $iNOS_{oxy}$ following exposure to NO. Again, the instantaneously formed 6C NO-bound enzyme with a Soret band at 439 nm converted to the 5C species with a Soret maximum at 390 nm and a single exponential decay rate of ~28 min, similar to that observed in the urea-stabilized monomeric wild-type enzyme sample. Similar kinetic behavior was observed with the K82A mutant (supplemental Fig. S3*b*), confirming that the 20–30-min kinetic phase originates from the monomeric form of the enzyme.

On the basis of these data, we concluded that NO binding to the ferric protein in either the monomeric or dimeric state instantaneously produces a 6C NO-bound ferric derivative with indistinguishable optical absorption spectra with a Soret transition maximum at 439 nm. Subsequently, the fast phase is attributed to the transition from the 6C NO-bound state of the monomeric protein ($[M–NO]_{6C}$) to the 5C species ($[M]_{5C\text{-}NO}$), whereas the slow phase is ascribed to the same reaction originating from the loose dimer ($[D–NO]_{6C}$) as described in Equation 1.

$$[D–NO]_{6C} \rightarrow [M–NO]_{6C} \rightarrow [M]_{5C\text{-}NO} \qquad \text{(Eq. 1)}$$

Here, the formation of the 5C species is rate-limited by the monomerization of the dimer with an apparent lifetime of ~300–400 min.

To gain insights into the nature of the 5C species, the NO-treated samples were examined by resonance Raman spectroscopy. As shown in Fig. 4, the resonance Raman spectra of the 5C species with a Soret maximum at 390 nm generated in the presence and absence of urea are very similar (*upper* and *middle traces*), indicating that the two 5C species are the same. Because these spectra are virtually identical to those of 5C NO-bound ferrous derivatives of a variety of heme proteins as characterized by the heme modes located at 349, 677, and 756 cm^{-1} and a broad Fe–NO stretching mode ($\upsilon_{Fe–NO}$) in the 520–526 cm^{-1} region (26–30), the resonance Raman spectrum of the 5C NO-bound ferrous derivative of the $iNOS_{oxy}$ complex was also obtained (Fig. 4, *lower trace*). Here, the 5C NO-bound ferrous derivative was formed by directly adding NO to the substrate- and cofactor-free ferrous enzyme because the conversion of the 6C ferrous NO complex to its 5C form has been demonstrated previously in both $iNOS_{oxy}$ and neuronal NOS_{oxy} by Stuehr and co-workers (31, 32). The small differences in the 378 and 524 cm^{-1} regions are attributed to differences in the contributions of the laser plasma lines. The identical features in the three traces shown in Fig. 4 indicate that exposure of the *ferric* derivative of H4B-free $iNOS_{oxy}$ to NO leads to the reduction of the ferric heme iron to the *ferrous* form and the breakage of the proximal iron–thiolate bond. According to Equation 1, the dimer-to-monomer conversion occurs prior to the reduction to the 5C ferrous form. This is consistent with prior reports of monomerization induced by the presence of NO, although we cannot exclude the less likely possibility of a direct reduction of the enzyme to the ferrous form prior to dissociation of the dimer.

To determine whether NO causes any chemical modifications of the polypeptide chain of $iNOS_{oxy}$, we carried out mass spectrometric measurements of the NO-treated samples. All samples examined were first subjected to trypsin digestion prior to mass spectrometric analysis. The major modification in the mass spectra of the NO-treated samples *versus* the control sample without NO treatment was the enhancement of the three fragment ions at *m*/*z* 581.94, 640.27, and 743.85 as shown in Fig. 5. The charge states of the three fragments were determined to be +3, +3, and +2, respectively, on the basis of their characteristic isotopic distributions. The parent masses of the ion peaks at *m*/*z* 581.94 and 743.85 (1742.82 and 1485.70 Da, respectively) calculated based on the charges are exact matches with two expected trypsin cleavage products of $iNOS_{oxy}$ corresponding to peptide fragments 82–97 and 393–404, respectively. These assignments were confirmed by the tandem mass spectrometric data (data not shown).

Intriguingly, all observed fragment ion peaks in the mass spectra can be accounted for by the expected trypsin cleavage products, except the triply charged ion at *m*/*z* 640.27 with a parent mass of 1917.81 Da. We found that this ion peak is an exact match of peptide fragments 98–105 and 108–117 disulfide bond-linked through Cys^{104} and Cys^{109}. This assignment was confirmed by the tandem mass data shown in supplemental Fig. S5. To further verify the disulfide-bonded peptide fragments, the trypsin-digested fragments of the NO-treated sample (in the presence of 4 M urea) were reduced by dithiothreitol (to reduce the disulfide bond) and alkylated by iodoacetamide (to alkylate the reduced free cysteine residues). This treatment resulted in the appearance of a doubly charged ion at *m*/*z* 553.76, the parent mass (1105.5 Da) of which is an exact match for peptide fragment 108–117 with a carbamidomethylated cysteine residue, at the expense of the fragment ion peak at *m*/*z* 640.27 (supplemental Fig. S6). The modified fragment 98–105 was not observed, possibly because of its low ionization propensity. These data further confirmed the presence of the disulfide-linked peptide fragment 98–105/108–117. It is important to note that, other than a very small contribution from a Cys^{109}–Cys^{109} disulfide-bonded fragment (data not shown), no other disulfide-linked trypsin-digested $iNOS_{oxy}$ fragments were observed; furthermore, no fragments were found to contain any NO-derivatized amino acids. This is in contrast to the results of NO treatment of nitrophorins, in which the proximal cysteine bond becomes ruptured and nitrosylated (33, 34).

Because the enzyme is in a monomeric state in the presence of 4 M urea, the formation of the disulfide-linked peptide fragment 98–105/108–117 must be a result of intramolecular rather than intermolecular interactions. Taken together, these data indicate that the NO-induced monomerization of the loose dimer is coupled to an intramolecular disulfide bond formation between cysteine residues at positions 104 and 109 and that the monomerization process exposes peptide fragments 82–97 and 393–404 to solvent,

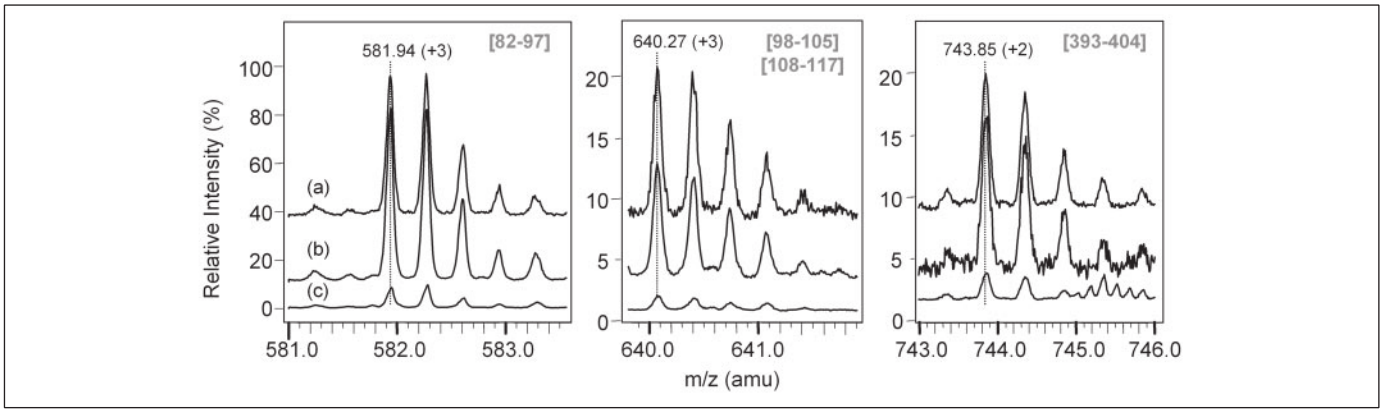

FIGURE 5. **Mass spectra of the NO-treated $iNOS_{oxy}$ samples with (*traces a*) and without (*traces b*) pretreatment with 4 M urea and the control sample without NO treatment (*traces c*).** All samples were digested with porcine trypsin for 12 h prior to the mass spectrometric measurements. The data show the three fragment ions (fragment 82–97, disulfide-linked fragment 98–105/108–117, and fragment 393–404) that underwent the largest change in intensity in response to the NO treatment. In each panel, the zero positions were displaced for clarity. The equally spaced peaks associated with each fragment are a result of hydrogen/deuterium isotopic substitution; based on the spacing, the charge state of each fragment ion was determined as indicated in *parentheses*. The identity of each fragment was confirmed by tandem mass spectrometry. *amu*, atomic mass units.

making them more accessible to trypsin digestion as reflected by the enhancement of the corresponding fragment ion peaks shown in Fig. 5.

DISCUSSION

The data presented here clearly demonstrate that, in the absence of H4B, the ferric derivative of $iNOS_{oxy}$ is in equilibrium between a monomeric state and a loose dimeric state. Furthermore, L-Arg binding to the enzyme shifts the equilibrium toward the loose dimeric state, whereas the addition of H4B locks the enzyme in a tight dimeric state that resists NO-induced monomerization. The NO-induced monomerization in the loose dimer is associated with the formation of an intramolecular disulfide bond between Cys^{104} and Cys^{109}, located in the zinc-binding motif in the dimer interface. The resulting monomeric enzyme with a 6C NO-bound heme iron gradually converts to a 5C NO-bound ferrous species because of the reduction of the heme iron and the concomitant breakage of the proximal iron–thiolate bond.

Autoreduction Mechanism—One possible mechanism to account for the conversion of the 6C NO-bound ferric derivative to the five-coordinate NO-bound ferrous form is a heterolytic cleavage of the proximal iron–thiolate bond: $Cys^{-}–Fe^{3+}–NO \rightarrow Cys^{\bullet} + Fe^{2+}–NO$. To test this mechanism, we re-examined the NO reaction with 4 M urea-treated $iNOS_{oxy}$ as a function of the NO concentration. We found that the formation rate of the 5C species increased approximately linearly as the NO concentration increased (data not shown). Because the S_n1-type heterolytic cleavage reaction predicts an NO concentration-independent kinetic process, this mechanism is excluded.

NO-mediated conversion of a 6C NO-bound ferric protein to a 6C NO-bound ferrous protein has been well documented for histidine-ligated heme proteins such as hemoglobin and myoglobin (35–37). In these cases, exposure of the ferric protein to NO first produces a 6C NO-bound ferric heme via displacement of the distal water ligand by NO (Equation 2).

$$His–Fe^{3+}–H_2O + NO \rightarrow His–Fe^{3+}–NO + H_2O \quad \text{(Eq. 2)}$$

The formation of the 6C NO-bound ferric heme is followed by autoreduction of the heme iron, leading to the formation of a 6C NO-bound ferrous heme. Three different mechanisms have been proposed to account for the NO-induced heme iron reduction reaction. In the first mechanism, proposed by Chien (35) and by Hoshino *et al.* (38), a base-catalyzed conversion of the 6C NO-bound ferric form to a nitrite-bound ferrous derivative ($His–Fe^{2+}–NO_2^-$) is followed by displacement of the heme-bound nitrite with a second NO molecule to form the NO-bound reduced heme ($His–Fe^{2+}–NO$). In the second mechanism, postulated by Ehrenberg and Szczepkowski (39), a rate-limiting heterolytic cleavage of the distal iron–NO bond, generating $His–Fe^{2+}$ and NO^+, is followed by coordination of a second NO molecule. In the third mechanism, proposed by Addison and Stephanos (36), the reduction of the NO-bound ferric heme is induced by nucleophilic attack by a second NO, resulting in a metastable species ($NO–Fe^{3+}–NO$), which rapidly converts to a ferrous form with the release of NO^+ and rebinding of the proximal His ligand.

In all three mechanisms, the reductant is the exogenous NO, which is oxidized to either a nitrite or a nitrosonium ion (NO^+). In a recent study, NO-induced autoreduction was observed in hemoglobin from a clam, *Scapharca inaequivalvis* (37). In that work, a 6C NO-bound *ferrous* species was observed instantaneously following the addition of NO to the *ferric* species. The authors proposed that the reaction follows the Addison and Stephanos (36) type of mechanism and that the absence of any detectable 6C NO-bound *ferric* derivative suggests that the overall reaction is rate-limited by the binding of NO to the ferric protein (Equation 2) instead of the following autoreduction reaction. More interestingly, it was shown that the nitrosonium ion (NO^+) released from the autoreduction reaction is able to nitrosylate a Cys residue to form an *S*-nitrosylated species (SNO).

On the basis of the current data, we postulate that monomeric 6C NO-bound ferric $iNOS_{oxy}$ is first reduced to the 6C NO-bound ferrous derivative by a mechanism similar to that proposed by Addison and Stephanos (36). Studies of the pH dependence of the reactions are needed to determine the contribution of the mechanism described by Chien (35) and Hoshino *et al.* (38). The formation of the ferrous derivative is followed by a homolytic cleavage of the proximal iron–thiolate bond to produce the 5C NO-bound ferrous species (Equations 3 and 4).

$$Cys^{-}–Fe^{3+}–NO + NO \rightarrow Cys^{-}–Fe^{2+}–NO + NO^{+} \quad \text{(Eq. 3)}$$

$$Cys^{-}–Fe^{2+}–NO \rightarrow Cys^{-} + Fe^{2+}–NO \quad \text{(Eq. 4)}$$

Because the 6C NO-bound ferrous derivative was not observed during the reaction, the reaction must be rate-limited by the autoreduction process described in Equation 3. This is consistent with the results reported by Abu-Soud *et al.* (31, 32), who found that, at 10 °C, the conversion of 6C NO-bound ferrous $iNOS_{oxy}$ to its 5C NO-bound derivative exhibits a lifetime of 4.6 min, which is much shorter than that

of the overall formation rate of the 5C species observed here. We propose that the NO^+ released from the autoreduction process can diffuse to the zinc-binding site and nitrosylate Cys^{104} or Cys^{109}, leading to intramolecular disulfide formation between these two residues, as will be discussed in more detail below. In a previous study (22), we reported that H4B binding to NO-bound ferric $iNOS_{oxy}$ brings about a significant out-of-plane distortion of the heme that perturbs the electronic properties of the heme iron, making it more difficult to reduce. The resistance of H4B-bound $iNOS_{oxy}$ to NO-induced autoreduction reported here can be attributed in part to the same origin.

Although it is well known that the 6C NO-bound ferric derivatives of myoglobin and hemoglobin are susceptible to autoreduction, the resulting 6C NO-bound ferrous species can be quite stable. On the other hand, the 6C NO-bound ferrous species found in several other heme protein systems, especially those involved in NO sensing and binding functions such as soluble guanylate cyclase (40), cytochrome *c′* (41), and other heme-based sensors (42), are labile. They readily convert to 5C NO-bound ferrous derivatives because of a weakened proximal iron–His bond. For thiolate-ligated heme protein systems such as cytochrome P450 and NOS (the H4B-bound form), the 6C NO-bound ferric complexes are typically more resistant to autoreduction because of the electron donating capability of the proximal cysteine thiolate that stabilizes the higher oxidation state of the heme iron. However, autoreduction and the associated breakage of the proximal iron–thiolate bond due to the changes in the electronic properties of the proximal thiolate ligand or the electrostatic environment of the distal NO-binding site have been reported in these protein systems. As an example, in cytochrome P450 1A2, Asp^{318} in the distal pocket stabilizes the NO-bound ferric complex by forming a hydrogen bond with the heme-bound NO. Exposure of the ferric derivative of the D318A mutant to NO results in a 5C NO-bound ferrous species (43). In NOS, a Trp residue on the proximal side of the heme, which forms a hydrogen bond with the sulfur atom of the proximal thiolate heme ligand, is very important in tuning the electron density on the thiolate ligand. NO exposure of the ferrous derivatives of neuronal NOS mutants in which this Trp residue is mutated to Tyr or Phe leads to the formation a 5C NO-bound ferrous species (44). The $iNOS_{oxy}$ data presented here provide an additional example in which NO binding to the ferric heme iron induces autoreduction of the heme iron as well cleavage of the proximal iron–thiolate bond.

Disulfide Bond Formation and the Mechanism of Monomerization—On the basis of the mass spectrometric data, we found that autoreduction of the heme iron and breakage of the proximal iron–thiolate bond in $iNOS_{oxy}$ are associated with intramolecular disulfide bond formation between Cys^{104} and Cys^{109}. Recently, Ravi *et al.* (20) reported that exposure of endothelial NOS to NO causes *S*-nitrosylation of a Cys residue in the zinc-binding site, leading to monomerization of the enzyme. *S*-Nitrosylation has also been reported in iNOS by Mitchell *et al.* (45). Although we did not find any evidence of nitrosylated cysteine residues in our NO-treated $iNOS_{oxy}$ samples by either optical absorption (as an increase in absorbance at ~320 nm) or mass spectrometry, we postulate that the disulfide bond formation is triggered by the nitrosylation of Cys^{104} and/or Cys^{109} by the NO^+ released from the autoreduction reaction as illustrated in Equation 5.

$$R_1S^- + R_2S^- + NO^+ \rightarrow R_1SNO + R_2S^- \rightarrow R_1S\text{–}SR_2 + NO^- \quad \text{(Eq. 5)}$$

In this model, one of the residues is *S*-nitrosylated (SNO), and the other thiolate attacks the thiol through an S_n2 type of reaction, resulting in the loss of nitroxyl and the formation of the disulfide bond. It is important to point out that, although NO^+ is a much better nitrosylation reagent than NO especially under the strictly anaerobic conditions applied here, we could not exclude the possibility of a direct reaction between neutral NO and the cysteine residues, as has been reported for several other protein systems (46–48). Nonetheless, based on either scenario, the disulfide bond is formed only in the monomeric or loose dimeric state when the two cysteine residues at positions 104 and 109 are accessible to NO^+/NO. It is important to point out that additional reactions may occur under aerobic conditions that also lead to disulfide bond formation (46–48); however, we view them as unlikely under our experimental conditions.

Based on the crystal structures shown in Fig. 1, the iNOS dimer is stabilized through the tetrahedral coordination of Cys^{104} and Cys^{109} to a zinc atom in an unswapped conformation or by forming a disulfide linkage between Cys^{109} residues in a swapped conformation in which the N-terminal β-hook interacts with a peptide segment from the opposite subunit. Because in all of our samples, including the controls, only a very small amount of the trypsin cleavage product contained an intermolecular Cys^{109}–Cys^{109} disulfide bond, the loose dimer samples we examined here are possibly in the unswapped conformation with zinc bound to the protein. To test this possibility, we measured the amount of zinc released by a PAR absorbance assay (20). Upon the conversion of $iNOS_{oxy}$ dimers to monomers, we found a quantitative release of zinc, confirming the presence of the unswapped configuration of our enzyme (supplemental Fig. S7). We postulate that the nitrosylation reaction of the cysteine residues and the consequent formation of the intramolecular Cys^{104}–Cys^{109} disulfide bonds trigger the dissociation of the NO-bound loose dimer into monomers, leading to the formation of the 5C NO-bound ferrous protein with the release of NO^+, which may further catalyze the monomerization reaction of the loose dimer. A similar disulfide bond formation reaction can also occur in the monomeric NO-bound state, resulting in the same 5C NO-bound ferrous product.

The results reported here establish a mechanistic basis for the dimer inhibitory effect of NO in iNOS reported by Chen *et al.* (16). The irreversible formation of the disulfide linkage induced by NO accounts for their following observations. 1) NO inhibits dimerization of iNOS monomers without causing heme release. 2) In the absence of H4B and L-Arg, NO irreversibly converts iNOS dimers to monomers. 3) Monomers thus formed do not dimerize when exposed to H4B and L-Arg, whereas NO has no effect on iNOS dimers preincubated with H4B and L-Arg. Furthermore, their data suggest that the disulfide bond formation reported here requires the pre-binding of NO to the sixth coordination site of the heme because the presence of a strong heme ligand (imidazole) prevents NO from inhibiting dimer formation. This hypothesis is currently under examination in our laboratory.

The side product of the disulfide bond reaction is the release of zinc. In iNOS, zinc has been proposed to act as a conformational switch between the swapped and unswapped conformations (Fig. 1) (17, 25). The NO-induced release of zinc in iNOS may thus play an important regulatory role. A similar NO-mediated release of thiolate-coordinated zinc has recently been implicated in a variety of protein systems (48–51), suggesting that the NO-linked intracellular signaling mechanism may be quite general. In NOS, this may be manifested in the iNOS system because its dimer stability is the weakest among the three isoforms (15).

Physiological Implications—Our results demonstrate a novel regulatory role of NO in $iNOS_{oxy}$ as illustrated in *red* and *green* in Fig. 6. On the basis of this model, when apo-iNOS is produced and released from the ribosome, it recruits a prosthetic heme group to form a monomeric holoprotein ($[M^{3+}]_{6C}$), which can assemble into a loose dimer ($[D'^{3+}]_{6C}$). In the absence of the substrate (L-Arg or *N*-hydroxyarginine) and cofactor (H4B), the loose dimer is in equilibrium with the mono-

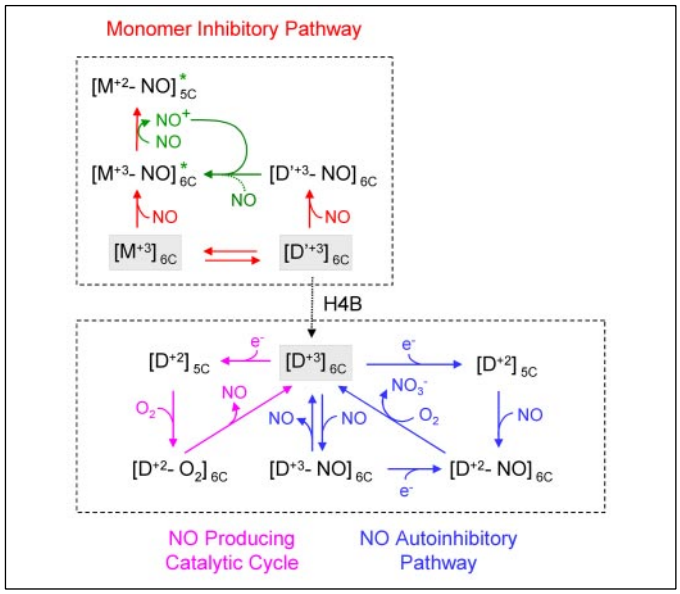

FIGURE 6. **Proposed NO-mediated regulatory mechanism in iNOS.** *M*, *D*, and *D′* represent the monomeric, tight dimeric, and loose dimeric forms of the enzyme, respectively. The *asterisks* indicate the presence of an intramolecular Cys^{104}–Cys^{109} disulfide bond. See "Discussion" for a full description.

meric state. L-Arg or *N*-hydroxyarginine binding shifts the equilibrium from the monomer toward the loose dimer, whereas H4B binding introduces conformational changes that convert the enzyme to the functional tight dimer ($[D^{3+}]_{6C}$). The NO generated in the tight dimer via the NO-producing catalytic cycle illustrated in *magenta* may bind to the freshly produced monomeric species ($[M^{3+}]_{6C}$) or the loose dimer ($[D'^{3+}]_{6C}$) to generate the 6C NO-bound species ($[M^{3+}–NO]^{*}_{6C}$ and ($[D'^{3+}–NO]_{6C}$, respectively). The monomeric 6C NO-bound species is not stable and readily converts to a 5C NO-bound ferrous species ($[M^{2+}–NO]^{*}_{5C}$) through autoreduction and the associated proximal iron–thiolate bond cleavage reaction. The autoreduction reaction produces a nitrosonium ion (NO^+), which may react with Cys^{104} and Cys^{109} in the monomer to form an *S*-nitrosylated product, which subsequently leads to an intramolecular disulfide bond between these two residues. The NO^+ can also react with the zinc-binding site of the loose dimer ($[D'^{3+}–NO]_{6C}$) via the same reaction, thereby inducing the monomerization of the dimer. A similar monomerization reaction may also be directly induced by the NO molecule as indicated by the *dotted green line* (although perhaps to a lesser extent).

The NO produced in the distal pocket of the tight dimer can also rebind to the heme iron to produce a 6C NO-bound ferric heme ($[D^{3+}–NO]_{6C}$) as indicated by the NO autoinhibitory pathway shown in *blue* in Fig. 6. If the 6C NO-bound ferric heme is reduced to the 6C NO-bound ferrous heme ($[D^{2+}–NO]_{6C}$) by receiving an electron from the reductase domain, the enzyme is trapped in this inactive state because the NO dissociation rate is very slow from the ferrous enzyme (the dissociation reaction is thus ignored in Fig. 6). When NO is overproduced, the $[D^{2+}–NO]_{6C}$ species can also be generated by NO binding to the ligand-free ferrous protein ($[D^{2+}]_{5C}$), although NO binding to the ferric heme is expected to be the dominant pathway. The $[D^{2+}–NO]_{6C}$ species can be converted back to the active $[D^{3+}]_{6C}$ state by reacting with O_2 to produce nitrate. It has been shown that the NO autoinhibitory pathway is regulated by a delicate balance between the dissociation rate of the NO, the reduction rate of the $[D^{3+}–NO]_{6C}$ species, and the nitration rate of $[D^{2+}–NO]_{6C}$ species with O_2 (52–54).

It is important to note that, in addition to the disulfide bond-mediated pathway described above, two additional dimer inhibition mechanisms have been shown to play an important role in limiting the amount of NO generated by iNOS in cells under physiological conditions. In the first mechanism, NO limits dimer assembly by preventing heme insertion and decreasing heme availability because heme is required for dimer formation. This mechanism was proposed based on a series of experiments conducted by Albakri and Stuehr (21) on iNOS induced in the RAW 264.7 mouse macrophage cell line. It was found that the endogenous production of NO down-regulated the formation of the dimers despite continued accumulation of the monomer. In the second mechanism, proteins that inhibit dimerization of iNOS by binding to its N terminus have been identified in both neuronal and macrophage cells. In macrophage cells, a physiological iNOS-specific dimerization inhibitor designated NAP110 (NOS-associated protein of 110 kDa) is up-regulated by interferon-γ and lipopolysaccharide *in vivo* (55). NAP110 binds to iNOS in the N-terminal region (residues 1–70), a region that is not homologous to the other isoforms, thereby selectively inhibiting its dimerization. Similarly, Kalirin, a large cytosolic protein with nine spectrin-like repeats, inhibits dimerization of iNOS in neuronal cells by binding to this same region (56). In both of these cases, the protein binds to iNOS monomers, but does not convert dimers back into the monomeric form. In view of the potential importance of the dimer inhibitory pathways, a number of highly selective synthetic iNOS dimerization inhibitors that show great therapeutic potential in iNOS-related pathologies have been developed (57, 58).

In summary, we have shown that NO can regulate the monomer-dimer equilibrium in iNOS by inducing the formation of a non-native disulfide linkage between Cys^{104} and Cys^{109}, in addition to its autoinhibitory effect. The novel monomer-dimer regulatory mechanism mediated by NO revealed here thus sheds new light on the functional mechanisms of NOS.

Acknowledgment—We thank Dr. Andy Arvai (Scripps Research Institute) for providing the coordinates for the crystal structures shown in Fig. 1.

REFERENCES

1. Stuehr, D. J. (1999) *Biochim. Biophys. Acta* **1411,** 217–230
2. Alderton, W. K., Cooper, C. E., and Knowles, R. G. (2001) *Biochem. J.* **357,** 593–615
3. Marletta, M. A. (1993) *Adv. Exp. Med. Biol.* **338,** 281–284
4. Nathan, C., and Xie, Q. W. (1994) *Cell* **78,** 915–918
5. Siddhanta, U., Presta, A., Fan, B., Wolan, D., Rousseau, D. L., and Stuehr, D. J. (1998) *J. Biol. Chem.* **273,** 18950–18958
6. Panda, K., Ghosh, S., and Stuehr, D. J. (2001) *J. Biol. Chem.* **276,** 23349–23356
7. Crane, B. R., Arvai, A. S., Ghosh, D. K., Wu, C., Getzoff, E. D., Stuehr, D. J., and Tainer, J. A. (1998) *Science* **279,** 2121–2126
8. Raman, C. S., Li, H., Martasek, P., Kral, V., Masters, B. S., and Poulos, T. L. (1998) *Cell* **95,** 939–950
9. Li, H., Raman, C. S., Glaser, C. B., Blasko, E., Young, T. A., Parkinson, J. F., Whitlow, M., and Poulos, T. L. (1999) *J. Biol. Chem.* **274,** 21276–21284
10. Fischmann, T. O., Hruza, A., Niu, X. D., Fossetta, J. D., Lunn, C. A., Dolphin, E., Prongay, A. J., Reichert, P., Lundell, D. J., Narula, S. K., and Weber, P. C. (1999) *Nat. Struct. Biol.* **6,** 233–242
11. Marletta, M. A. (1994) *Cell* **78,** 927–930
12. Klatt, P., Schmidt, K., Lehner, D., Glatter, O., Bachinger, H. P., and Mayer, B. (1995) *EMBO J.* **14,** 3687–3695
13. Klatt, P., Pfeiffer, S., List, B. M., Lehner, D., Glatter, O., Bachinger, H. P., Werner, E. R., Schmidt, K., and Mayer, B. (1996) *J. Biol. Chem.* **271,** 7336–7342
14. Mayer, B., Wu, C., Gorren, A. C., Pfeiffer, S., Schmidt, K., Clark, P., Stuehr, D. J., and Werner, E. R. (1997) *Biochemistry* **36,** 8422–8427
15. Panda, K., Rosenfeld, R. J., Ghosh, S., Meade, A. L., Getzoff, E. D., and Stuehr, D. J. (2002) *J. Biol. Chem.* **277,** 31020–31030
16. Chen, Y., Panda, K., and Stuehr, D. J. (2002) *Biochemistry* **41,** 4618–4625
17. Crane, B. R., Rosenfeld, R. J., Arvai, A. S., Ghosh, D. K., Ghosh, S., Tainer, J. A., Stuehr, D. J., and Getzoff, E. D. (1999) *EMBO J.* **18,** 6271–6281
18. Abu-Soud, H. M., Wang, J., Rousseau, D. L., Fukuto, J. M., Ignarro, L. J., and Stuehr, D. J. (1995) *J. Biol. Chem.* **270,** 22997–23006
19. Abu-Soud, H. M., Ichimori, K., Nakazawa, H., and Stuehr, D. J. (2001) *Biochemistry*

40, 6876–6881
20. Ravi, K., Brennan, L. A., Levic, S., Ross, P. A., and Black, S. M. (2004) *Proc. Natl. Acad. Sci. U. S. A.* **101,** 2619–2624
21. Albakri, Q. A., and Stuehr, D. J. (1996) *J. Biol. Chem.* **271,** 5414–5421
22. Li, D., Stuehr, D. J., Yeh, S.-R., and Rousseau, D. L. (2004) *J. Biol. Chem.* **279,** 26489–26499
23. Miller, R. T., Martasek, P., Raman, C. S., and Masters, B. S. (1999) *J. Biol. Chem.* **274,** 14537–14540
24. Wang, J., Rousseau, D. L., Abu-Soud, H. M., and Stuehr, D. J. (1994) *Proc. Natl. Acad. Sci. U. S. A.* **91,** 10512–10516
25. Ghosh, D. K., Crane, B. R., Ghosh, S., Wolan, D., Gachhui, R., Crooks, C., Presta, A., Tainer, J. A., Getzoff, E. D., and Stuehr, D. J. (1999) *EMBO J.* **18,** 6260–6270
26. Deinum, G., Stone, J. R., Babcock, G. T., and Marletta, M. A. (1996) *Biochemistry* **35,** 1540–1547
27. Vogel, K. M., Hu, S., Spiro, T. G., Dierks, E. A., Yu, A. E., and Burstyn, J. N. (1999) *J. Biol. Inorg. Chem.* **4,** 804–813
28. Andrew, C. R., Green, E. L., Lawson, D. M., and Eady, R. R. (2001) *Biochemistry* **40,** 4115–4122
29. Reynolds, M. F., Parks, R. B., Burstyn, J. N., Shelver, D., Thorsteinsson, M. V., Kerby, R. L., Roberts, G. P., Vogel, K. M., and Spiro, T. G. (2000) *Biochemistry* **39,** 388–396
30. Lukat-Rodgers, G. S., and Rodgers, K. R. (1997) *Biochemistry* **36,** 4178–4187
31. Abu-Soud, H. M., Wu, C., Ghosh, D. K., and Stuehr, D. J. (1998) *Biochemistry* **37,** 3777–3786
32. Huang, L., Abu-Soud, H. M., Hille, R., and Stuehr, D. J. (1999) *Biochemistry* **38,** 1912–1920
33. Weichsel, A., Maes, E. M., Andersen, J. F., Valenzuela, J. G., Shokhireva, T., Walker, F. A., and Montfort, W. R. (2005) *Proc. Natl. Acad. Sci. U. S. A.* **102,** 594–599
34. Walker, F. A. (2005) *J. Inorg. Biochem.* **99,** 216–236
35. Chien, J. C. (1969) *J. Am. Chem. Soc.* **91,** 2166–2168
36. Addison, A. W., and Stephanos, J. J. (1986) *Biochemistry* **25,** 4104–4113
37. Boffi, A., Sarti, P., Amiconi, G., and Chiancone, E. (2002) *Biophys. Chem.* **98,** 209–216
38. Hoshino, M., Maeda, M., Konishi, R., Seki, H., and Ford, P. C. (1996) *J. Am. Chem. Soc.* **118,** 5702–5707
39. Ehrenberg, A., and Szczepkowski, T. W. (1960) *Acta Chem. Scand.* **14,** 1684–1692
40. Stone, J. R., and Marletta, M. A. (1996) *Biochemistry* **35,** 1093–1099
41. Lawson, D. M., Stevenson, C. E., Andrew, C. R., and Eady, R. R. (2000) *EMBO J.* **19,** 5661–5671
42. Karow, D. S., Pan, D., Tran, R., Pellicena, P., Presley, A., Mathies, R. A., and Marletta, M. A. (2004) *Biochemistry* **43,** 10203–10211
43. Nakano, R., Sato, H., Watanabe, A., Ito, O., and Shimizu, T. (1996) *J. Biol. Chem.* **271,** 8570–8574
44. Voegtle, H. L., Sono, M., Adak, S., Pond, A. E., Tomita, T., Perera, R., Goodin, D. B., Ikeda-Saito, M., Stuehr, D. J., and Dawson, J. H. (2003) *Biochemistry* **42,** 2475–2484
45. Mitchell, D. A., Erwin, P. A., Michel, T., and Marletta, M. A. (2005) *Biochemistry* **44,** 4636–4647
46. Pryor, W. A., Church, D. F., Govindan, C. K., and Crank, G. (1982) *J. Org. Chem.* **47,** 156–159
47. Gow, A. J., Buerk, D. G., and Ischiropoulos, H. (1997) *J. Biol. Chem.* **272,** 2841–2845
48. Aravindakumar, C. T., Ceulemans, J., and De Ley, M. (1999) *Biochem. J.* **344,** 253–258
49. Kroncke, K. D., Suschek, C. V., and Kolb-Bachofen, V. (2000) *Antioxid. Redox Signal.* **2,** 585–605
50. Binet, M. R., Cruz-Ramos, H., Laver, J., Hughes, M. N., and Poole, R. K. (2002) *FEMS Microbiol. Lett.* **213,** 121–126
51. Spahl, D. U., Berendji-Grun, D., Suschek, C. V., Kolb-Bachofen, V., and Kroncke, K. D. (2003) *Proc. Natl. Acad. Sci. U. S. A.* **100,** 13952–13957
52. Santolini, J., Meade, A. L., and Stuehr, D. J. (2001) *J. Biol. Chem.* **276,** 48887–48898
53. Stuehr, D. J., Santolini, J., Wang, Z. Q., Wei, C. C., and Adak, S. (2004) *J. Biol. Chem.* **279,** 36167–36170
54. Gautier, C., Negrerie, M., Wang, Z. Q., Lambry, J. C., Stuehr, D. J., Collin, F., Martin, J. L., and Slama-Schwok, A. (2004) *J. Biol. Chem.* **279,** 4358–4365
55. Ratovitski, E. A., Bao, C., Quick, R. A., McMillan, A., Kozlovsky, C., and Lowenstein, C. J. (1999) *J. Biol. Chem.* **274,** 30250–30257
56. Ratovitski, E. A., Alam, M. R., Quick, R. A., McMillan, A., Bao, C., Kozlovsky, C., Hand, T. A., Johnson, R. C., Mains, R. E., Eipper, B. A., and Lowenstein, C. J. (1999) *J. Biol. Chem.* **274,** 993–999
57. Blasko, E., Glaser, C. B., Devlin, J. J., Xia, W., Feldman, R. I., Polokoff, M. A., Phillips, G. B., Whitlow, M., Auld, D. S., McMillan, K., Ghosh, S., Stuehr, D. J., and Parkinson, J. F. (2002) *J. Biol. Chem.* **277,** 295–302
58. Kolodziejski, P. J., Koo, J. S., and Eissa, N. T. (2004) *Proc. Natl. Acad. Sci. U. S. A.* **101,** 18141–18146